Communications in Physics, Vol. 32, No. 3 (2022), pp. 285-293
DOI: https://doi.org/10.15625/0868-3166/16597

$Mn_{55-x}Co_xBi_{45}$ MELT SPUN RIBBONS: MICROSTRUCTURES AND MAGNETIC PROPERTIES

TRUONG XUAN NGUYEN[1,†], ANH KHA VUONG[2], NGAN THUY THI DANG[1], NAM HOAI NGUYEN[1], NAM HONG PHAM[1], NGUYEN VAN QUYNH[3], DINH VAN TUAN[4] AND VUONG VAN NGUYEN[1]

[1]*Institute of Materials Science, Vietnam Academy of Science and Technology, No.18, Hoang Quoc Viet Road, Cau Giay district, Hanoi, Vietnam*

[2]*Faculty of pedagogy, Ha Noi Metropolitan University, No. 98, Duong Quang Ham road, Cau Giay District, Hanoi, Vietnam*

[3]*University of Science and Technology of Hanoi, Vietnam Academy of Science and Technology, No. 18, Hoang Quoc Viet road, Cau Giay District, Hanoi, Vietnam*

[4]*Electric Power University, No. 235, Hoang Quoc Viet road, Cau Giay District, Hanoi, Vietnam*

E-mail: †truongnx@ims.vast.vn

Received 4˚Ctober 2021; *Accepted for publication 12 February 2022*; *Published 30 May 2022*

Abstract. *In this paper, we present the effect of Cobalt (Co) addition on the crystallization, microstructures and magnetic properties of $Mn_{55-x}Co_xBi_{45}$ ($x = 0,\ 5,\ 10,\ 20$) melt - spun ribbons. The ribbons were prepared by the melt-spinning technique and subsequent anneal at 280˚C for 5 h. The samples were investigated by using X-ray diffraction (XRD), Differential Scanning Calorimetry (DSC) traces as well the Vibration Sample Magnetometer (VSM) measurements. The obtained results prove that 5% at. of Co-content added to the MnBi system is the optimal. The larger Co content causes the eutectic Mn-Co formation which restricts the reaction between Mn and Bi to form MnBi ferromagnetic phase responsible for ribbons's saturation magnetization Ms. The highest magnetization Ms of 65 emu/g and the coercivity ${}_iH_c$ of 4.7 kOe were achieved for the ribbon of $Mn_{50}Co_5Bi_{45}$. The effect of Co content on the microstructures and magnetic properties of $Mn_{55-x}Co_xBi_{45}$ melt - spun ribbons are discussed in detail.*

Keywords: melt - spun ribbons; microstructures; XRD patterns; DSC traces; VSM hysteresis loops; magnetic properties.

Classification numbers: 61.72.-y; 75.60.Ch.

I. INTRODUCTION

Since the early 1950s, MnBi-based magnets were investigated [1], however, over the past 70 years the energy product (BH)max value of MnBi bulk magnets is restricted at 8.4 MGOe [2] that is only a half of the theoretical limit of 17.6 MGOe [3]. The MnBi material shows the morderate spontaneous magnetization Ms of ~ 8.2 kG, the high magneto-crystalline energy Ka of 0.9 MJ/m^3, the elevated Curie temperature Tc of 360˚C and specially the positive temperature coefficient of coercivity $d({}_iH_c)/dT > 0$. These features make MnBi-based magnets prospective for high-temperature applications [4] and therefore their processing is continuouly developed.

The specific feature of MnBi alloys is the multi-phase (MnBi, Mn, Bi) caused by the peritectic solidification that requires an anneal process for enhancing the MnBi content. Unfortunately, due to the low formation temperature Tf of the ferromagnetic phase of MnBi ($T_f < 340$˚C thus it is named as the Low - Temperature Phase – MnBi LTP), the annealing temperature Ta must be < 340˚C and thus, the annealing time ta should be of several tens of hours [2, 3, 5]. After annealing, Ms is improved significantly, but the intrinsic coercivity ${}_iH_c$ is low $\sim 1 - 2$ kOe because of the long-time grain growth during the annealing. To avoid the peritectic solidification and to enhance iHc, the melt-spinning technique was applied for fabricating Mn_xBi_{100-x} ribbons, where the molten Mn_xBi_{100-x} alloys are ejected and quickly undercooled on the surface of the rotating copper wheel. This method allows preparing the ribbons of high MnBi LTP-content balanced with large ${}_iH_c$ by using the undercooling crystalline growth process managed by the cooling rate controlled by changing the wheel speed v_w. Yang et al. [6, 7] had prepared an amorphous MnBi ribbons at $v_w = 65$ m/s, then the MnBi ribbons were annealed at 260 - 320˚C to increase LTP MnBi content up to 95 %wt and ${}_iH_c = 3$ kOe. In this work, the annealing time was not reported. It is understood that the amorphous ribbons anneal is a delicate process that must simultaneously enhance the LTP content and keep ${}_iH_c$ high, so the balance between magnetization and coercivity of ribbons is not easily controlled and the energy product of ribbons is not well governed.

However, the melt-spinning process can be utilized with an optimized wheel speed to prepare the crystallized ribbons with compositions and microstructures creating a good Mr-bHc balance. So, the crystallized melt-spun MnBi ribbons can be immediately used to prepare green powders used in making high performance MnBi bulk magnets [7–14]. In this paper, we utilize the melt-spinning process with an appropriate wheel speed to prepare crystallized MnBi ribbons with the sequent annealing process. To control Ms of ribbons we add Cobalt element to MnBi in the composition of $Mn_{55-x}Co_xBi_{45}$ with $x = 0$, 5, 10 and 20. The evolution of LTP phase with doping Co, the microstructure and magnetic properties of prepared ribbons will be discussed in detail.

II. EXPERIMENTS

The chosen alloys of $Mn_{55-x}Co_xBi_{45}$ (x = 0, 5, 10, 20) were arc-melted from high-purity metals Mn and Co of 99.9%, and Bi of 99.99% under protection of argon atmosphere. The ingots were melted five times with controlling the arc-current to avoid any evaporation of Mn and Bi (the batch mass loss was < 0.3 %wt.). These pre-alloys were remelted in a high-quality quartz tube of the melt-spinner and ejected onto a rotating cooper wheel in 0.05 MPa argon atmosphere. The batchs of pre-alloys were kept around 15 g. The wheel speed was chosen at the optimized value of 20 m/s, the quartz tube orifice diameter was fixed at 0.8 mm, the distance between the nozzle

and the wheel surface was kept about 3 mm. The melt-spun ribbons were annealed at $280 \pm 5^{\circ}$C in argon for different times ranged up to 5 h. The XRD patterns of as-spun and annealed ribbons were carried out by using D8 advance Brucker X-ray diffractometer with Cu-K_α radiation with the scattering 2λ angle scan in the range from 20 to 80 degrees by the scanning step of 0.05° for 5s. The phase compositions of ribbons were analyzed by using the Rietveld refinement method. The MnBi LTP content γ of ribbons is determined by using the ratio α between the intensities of the peaks of MnBi(101) and Bi(012), $\alpha = (I_{MnBi}(101)/I_{Bi}(012))$, of their XRD patterns [15]. The DSC traces of ribbons were measured by Labsys Evo system at a chosen temperature profile in pure argon flow to check the ribbons' phases. The particles sizes of ball-milled ribbons were estimated by using Hitachi-S4800 field emission scanning electron microscopy (FESEM). The magnetic properties of prepared ribbons were evaluated from their hysteresis loops measured by the Vibrating sample magnetometer (VSM MicroSence).

III. RESULTS AND DISCUSSION

III.1. Microstructures and magnetic properties of $Mn_{55-x}Co_xBi_{45}$ as-spun ribbons

The XRD patterns of $Mn_{55-x}Co_xBi_{45}$ ($x = 0$, 5, 10, 20) ribbons melt-spun at the wheel speed of 20 m/s were shown in Fig. 1. The main phases of MnBi, Bi were marked on the diagram Fig. 1(a) for the MnBi ribbon. The XRD diagrams Figs. 1 (b) and 1(c) of the ribbons with $x = 5$ and 10 show the peak of bcc-Co located at 44.5° together with MnBi and Bi peaks. One notes that, together with MnBi, Bi and Co phases the diagram Fig. 1(d) is featured by the peak appeared at around 43° which is identified for the phase of $Mn_\alpha Co_\beta$ eutectic alloy. At $x = 0$, the MnBi LTP content $\gamma = 22.4$ wt.%. By increasing x, γ changes not monotonously and equals 16.9, 28.9 and 2.1 wt.% for $x = 5$, 10 and 20, respectively.

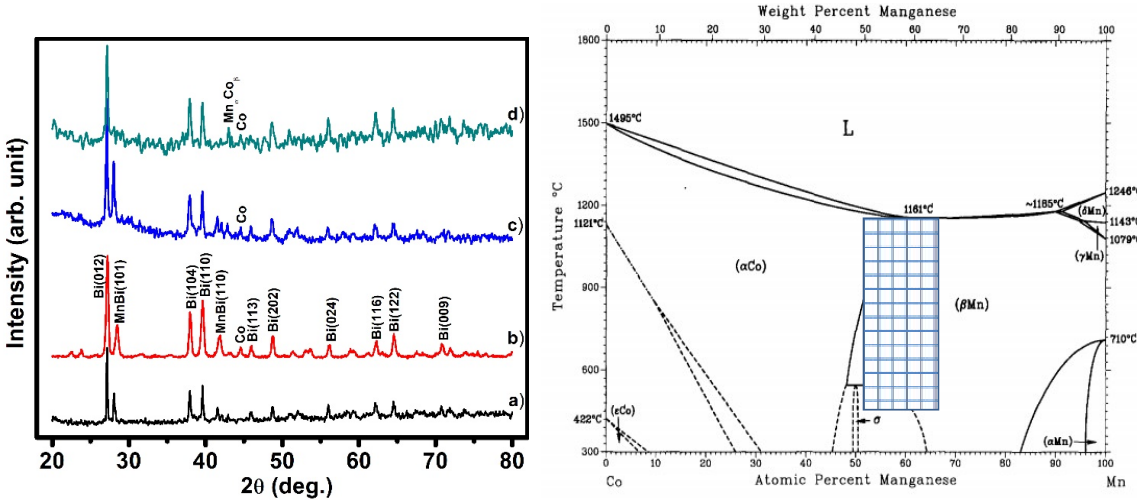

Fig. 1. (Left): XRD patterns of $Mn_{55-x}Co_xBi_{45}$ as-spun ribbons: a) $x = 0$; b) $x = 5$; c) $x = 10$; d) $x = 20$. (Right): Mn-Co phase diagram [15], the squared area marks the window where the Mn-Co eutectic phase can be formed.

The appearances of bcc-Co and $Mn_\alpha Co_\beta$ peaks reveal the presence of Co added to MnBi system and the reaction between added Co and Mn to form a eutectic alloy during the quenching process. By increasing x value, the amounts of Mn and Co fall into the window of the eutectic alloys Mn-Co marked by the squared area on the Mn-Co binary phase diagram cited from Ref. [15] and plotted on the right side of Fig. 1. The solidification of ribbons˚Ccurs at the undercooling state with the possible reactions Mn+Bi, Mn+Co, MnBi+Co and MnBi+ $Mn_\alpha Co_\beta$. For $x = 10$, the relative ratio Mn/Co is 81.8/18.2, and that of Mn/Bi is 50/50. Despite the ratio Mn/Co lays on the right side of the window of Mn-Co eutectic alloys, the ratio 50/50 of Mn/Bi leads to the preferred reaction Mn+Bi to form MnBi LTP followed by the weak reaction MnBi+Co. This situation stays valid for $x < 10$ and lead to the XRD patterns Fig. 1 (b,c). However, for $x = 20$, the circumstance is changed critically. The relative ratio Mn/Bi = 43.7/56.3 is far from the stoichiometric relation of $Mn_{50}Bi_{50}$ and weakens the MnBi LTP formation. In addition, the reaction between Mn and Co is eutectic, the formation of which is very strong in comparison with the peritectic reaction between Mn and Bi, so on the XRD pattern Fig. 1(d) one observes the peaks Co, $Mn_\alpha Co_\beta$ without the peak of MnBi LTP. So, before touching the surface of the copper wheel, inside the molten drops Mn reacts with Co forming the eutectic alloy and this eutectic alloy prevents the combination between Mn and Bi resulting in the absence of the MnBi LTP on the XRD diagram Fig. 1(d).

The evolution of the MnBi LTP formation of $Mn_{55-x}Co_xBi_{45}$ ($x = 0$, 5, 10 and 20) samples were investigated by the DSC traces scanned by the speed of 10˚C/min (see Fig. 2). For $Mn_{55}Bi_{45}$ ribbon, the first endothermic peak located at 268˚C relates with the melt of the eutectic composition $Bi_{98}Mn_2$ [16], the second one located at 352˚C corresponds to the Curie temperature where the ferromagnetic phase transforms to the paramagnetic one [17].

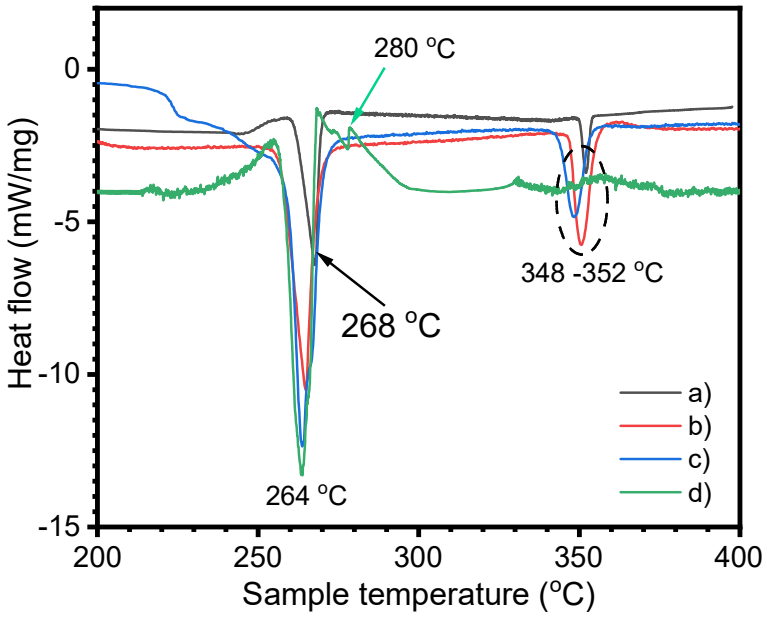

Fig. 2. (color online) The DSC traces scanned by 10˚C/min of $Mn_{55-x}Co_xBi_{45}$ as spun ribbons: a) $x = 0$; b) $x = 5$; c) $x = 10$; d) $x = 20$.

For $Mn_{55-x}Co_xBi_{45}$ ribbons, the first endothermic peaks were shifted to the lower temperature and located at about 264˚C. The second endothermic peaks corresponding to the Curie temperature Tc are also located at lower temperatures, at 350˚C and 348˚C for $x = 5$ and 10, respectively. The exothermic peak located at 280˚C on the DSC trace of the ribbon with $x = 20$ at.% (see Fig. 2d) reveals the crystallization of Mn-Co eutectic alloy which prevents the reaction between Mn and Bi to form MnBi LTP, so the MnBi LTP in this ribbon is very low resulting the disappearance of the peak located around 350˚C on its DSC trace and of the XRD peak MnBi(101) on the XRD diagram Fig. 1d. This fact is supported also by calculating the value of latent heat (L) of the first endothermic peaks located at 264 – 268˚C. This value is increased by increasing Co content ($L = 5.54$ J/g for $x = 0$ and $L = 12.68$ J/g as $x = 20$) which means the content of the free bismuth is large with larger value of x caused by the absence of Mn-Bi combination.

During the rapid quench, the MnBi LTP is formed together with the Mn and Bi inclusions as a result of the combination between them. Since the period at which the ribbons are held at the temperature T below 340˚C is very short, so the micrometer-sized Mn and Bi inclusions seem huge to combine one with another to form MnBi and thus to result in the low values of MnBi LTP contents of ribbons. Depending on the MnBi LTP as the ferromagnetic phase, the magnetic properties of $Mn_{55-x}Co_xBi_{45}$ (x = 0, 5, 10 and 20) as-spun ribbons were changed. The Ms and ${}_iH_c$ values of these ribbons were measured by VSM (not shown here) and are summarized in Table 1. The maximum magnetization Ms (magnetization measured at 20 kOe field) of ribbons decrease from 15.3 to 1.6 emu/g by increasing Co from 0 to 20 at% in correlation with the MnBi LTP contents of these ribbons. The maximum ${}_iH_c$ of 8.2 kOe is obtained for the ribbon with $x = 5$ at.% Co.

Table 1. Summary of magnetic properties estimated from the VSM loops of $Mn_{55-x}Co_xBi_{45}$ (x = 0, 5, 10 and 20) as-spun ribbons.

x (at.% Co)	M_s (emu/g)	H_c (kOe)
0	15.3	5.3
5	12.5	8.2
10	4.8	6.7
20	1.6	5.5

III.2. The phase evolution and magnetic properties of $Mn_{55-x}Co_xBi_{45}$ annealed spun ribbons

To enhance the MnBi LTP contents, the $Mn_{55-x}Co_xBi_{45}$ ($x = 0$, 5, 10 and 20) as-spun ribbons were annealed at 280 ˚ C in the argon flow for 5 h [18, 19]. The handly crushed powders were subjected to the in-xylene low energy ball-milling process for 120 min by using the hard steel 6 mm diameter balls with the weight ratio balls to powders 10:1. Fig. 3 show FESEM images of ball-milled powder of $Mn_{55-x}Co_xBi_{45}$ ($x = 0$, 5, 10 and 20) annealed ribbons. The grain sizes are of 4 - 5 μm for $x = 0$ and 5 at.% and 7 - 8 μm for $x = 10$, 20 at.%. These discrete values mean that by x over the value of 5% at, the behavior of Co entering to the MnBi system changes abruptly involving the change in mechanical properties of $Mn_{55-x}Co_xBi_{45}$.

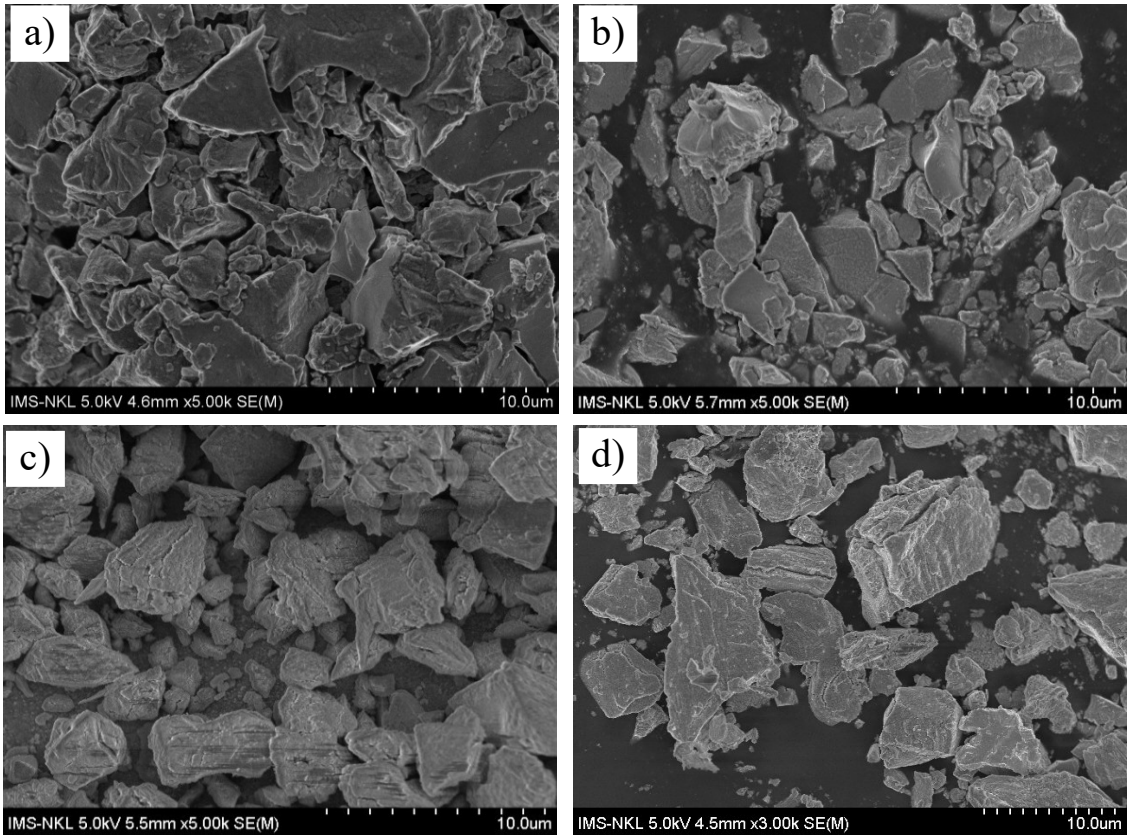

Fig. 3. FESEM images of $Mn_{55-x}Co_xBi_{45}$ crushed powders: a) $x = 0$; b) $x = 5$; c) $x = 10$; d) $x = 20$.

The XRD patterns plotted in Fig. 4 show the significant enhancement of MnBi LTP content obtained by the above mentioned aneal. Almost the peaks appeared on the diagrams Fig. 4a, b, c belong to the MnBi LTP except the peaks of Bi(012) and (Bi(015).

The ratios between two strongest peaks of MnBi and Bi (see Fig. 4), $\alpha = I_{\mathrm{MnBi101)}}/I_{\mathrm{Bi102}}$), allow to estimate the MnBi LTP contents equal 80, 85, 70 and 45 wt% for the $Mn_{55-x}Co_xBi_{45}$ ribbons with $x = 0$, 5, 10 and 20, respectively. One notes that, the ribbon $Mn_{55-x}Co_xBi_{45}$ with $x = 0$ and 5 are featured by the clear peak appearances revealing the good growth of MnBi LTP governed by the applied annealing process. For the ribbons with larger content of Co, $x = 10$ and 20, because of the presence of the eutectic Mn-Co phase mentioned above, the crystal growth of MnBi LTP was worse and together with MnBi and Bi peaks one also observes the star-marked peak which is not identified but probably resulted from the reaction between the eutectic alloy $Mn_\alpha Co_\beta$ and Bi during the applied annealing process.

Corresponding to the MnBi LTP contents predicted from the XRD diagrams, the ball-milled micrometer sized annealed powders shown by SEM graphs have the hysteresis loops plotted in Fig. 5. The maximum magnetization of ribbons with $x = 5$ at.% has the highest value of 65 emu/g

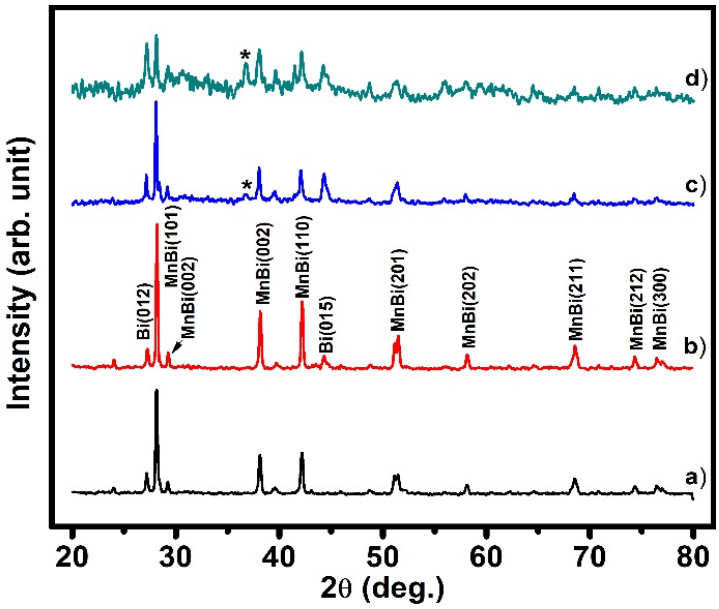

Fig. 4. XRD patterns of $Mn_{55-x}Co_xBi_{45}$ annealed ribbons: a) $x = 0$; b) $x = 5$; c) $x = 10$; d) $x = 20$.

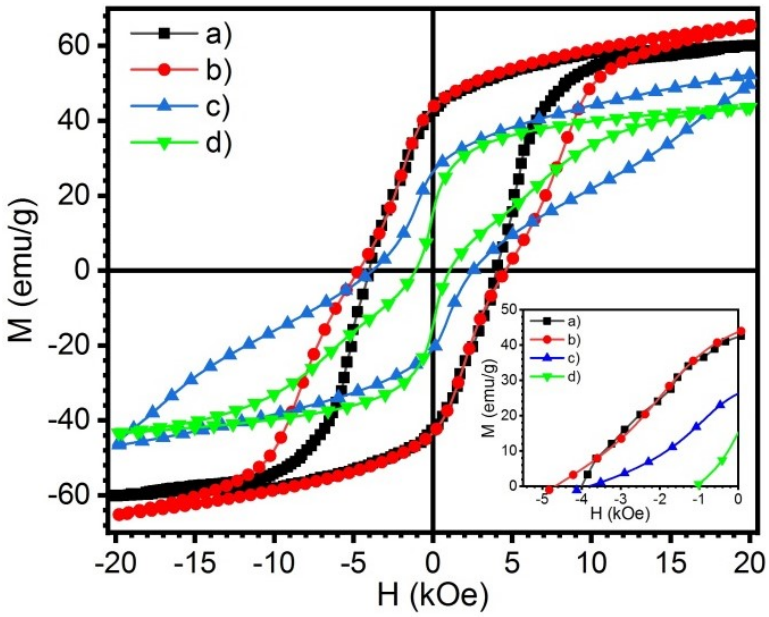

Fig. 5. The M(H) curves of $Mn_{55-x}Co_xBi_{45}$ annealed ribbons: a) $x = 0$; b) $x = 5$; c) $x = 10$; d) $x = 20$. The insert shows the 2nd branch of M(H) loops of ribbons.

against 59, 50 and 43 emu/g for the ribbons with $x = 0$, 10 and 20 at.%. This magnetization value agrees with the value of 85 wt% of MnBi LTP content determined from the XRD patterns plotted in Fig. 5 and corresponds to the value of $M_s = 74$ emu/g measured by PPMS in 90 kOe field presented in Ref. [2]. It is worthy to note that the ribbon with the highest magnetization owns at the same time the largest coercivity of 4.7 kOe and the smooth loop branch in the 2nd quadrant. These values are estimated from the minor loop measured by the maximal measuring field of 20 kOe and for the isotropic sample made from the ball-milled powders without any in-field alignment. By increasing the Co addition values the magnetizations and coercivities are decreased and the loops are kinked, which relate with the phase compositions discussed above from the XRD diagrams plotted on Fig. 4.

IV. CONCLUSION

The paper presents and discusses the preparation and MnBiLTP formation as well the magnetic performance of Co-added $Mn_{55-x}Co_xBi_{45}$ ($x = 0$, 5, 10 and 20) ribbons melt-spun using the conventional commercial rapid quench furnace ZGK-1, followed by the subsequent annealing at 280˚C for 5 h. The obtained results reveal that the Co addition to the MnBi system is a complex process and the optimal value of Co added to the MnBi system is in the range of 5 – 10 at.%, over which the reaction between Mn and Co to form eutectic Mn-Co alloy is˚Ccurred to prevent the MnBiLTP formation. The highest values of magnetization and coercivity are 65 emu/g and 4.7 kOe for the isotropic powder ball-milled from $Mn_{50}Co_5Bi_{45}$ ribbon. The optimization of ribbon microstructures to improve the coercivity should enhance the kink behavior and sequentially the ribbon energy product (BH)max to the value of around 8 — 9 MGOe that should be enough to use ribbons for making MnBi bonded magnets.

ACKNOWLEDGEMENT

We grateful acknowledge financial support from the Vietnamese Ministry of Science and Technology (MOST) under project NĐT/CN/21/25.

REFERENCES

[1] E. Adams, W. M. Hubbard and A. M. Syeles, *A new permanent magnet from powdered manganese bismuthide*, *J. Appl. Phys.* **23** (1952) 1207.

[2] Van Vuong Nguyen, N. Poudyal, X. Liu, J. P. Liu, Kewei Sun, M. J. Kramer and J. Cui, *High-performance MnBi alloy prepared using profiled heat treatment*, *IEEE Trans. Magn.* **50** (2014) 1.

[3] J. Cui, J. P. Choi, G. Li, E. Polikarpov, J. Darsell, N. Overman, M. Olszta, D. Schreiber, M. Bowden, T. Droubay, M. J. Kramer, N. A. Zarkevich, L. L. Wang, D. D. Johnson, M. Marinescu, I. Takeuchi, Q. Z. Huang, H. Wu, H. Reeve, N. V. Vuong, J. P. Liu, *Thermal stability of MnBi magnetic materials*, *J. Phys. Condens. Matter* **26** (2014) 064212.

[4] J. M. D. Coey, *New permanent magnets; manganese compounds*, *J. Phys. Condens. Matter* **26** (2014) 064211.

[5] N. V. Vuong and N. X. Truong, *Low temperature phase of the rare-earth-free MnBi magnetic material*, *Vietnam J. Sci. Technol.* **54** (1A) (2016) 50.

[6] Y. B. Yang, X. G. Chen, R. Wu, J. Z. Wei, X. B. Ma, J. Z. Han, H. L. Du, S. Q. Liu, C. S. Wang, Y. C. Yang, Y. Zhang and J. B. Yang, *Preparation and magnetic properties of MnBi*, *J. Appl. Phys.* **111** (2012) 07E312.

[7] Y. B. Yang, X. G. Chen, S. Guo, A. R. Yan, Q. Z. Huang, M. M. Wu, D. F. Chen, Y. C. Yang and J. B. Yang, *Temperature dependences of structure and coercivity for melt-spun MnBi compound*, *J. Magn. Magn. Mater.* **330** (2013) 106.

[8] C. S. Lakshmi and R. W. Smith, *Structural and magnetic properties of rapidly quenched Bi-Mn alloys*, *Mater. Sci. Eng. A* **133** (1991) 241.
[9] X. Guo, Z. Altounian, and J. O. Ström-Olsen, *Formation of MnBi ferromagnetic phases through crystallization of the amorphous phase*, *J. Appl. Phys.* **69** (1991) 6067.
[10] K. Kanga, L. H. Lewis and A. R. Moodenbaugh, *Crystal structure and magnetic properties of MnBi–Bi nanocomposite*, *J. Appl. Phys.* **97** (2005) 10K302.
[11] X. Guo, X. Chen, Z. Altounian and J. O. Ström-Olsen, *Magnetic properties of MnBi prepared by rapid solidification*, *Phys. Rev. B* **46** (1992) 14578.
[12] D. T. Zhang, W. T. Geng, M. Yue, W. Q. Liu, J. X. Zhang, J. A. Sundararajan and Y. Qiang, *Crystal structure and magnetic properties of* Mn_xBi_{100-x} *(*$x = 48$*,* 50*,* 55 *and* 60*) compounds*, *J. Magn. Magn. Mater.* **324** (2012) 1887.
[13] Tetsuji Saito, Ryuji Nishimura and Daisuke Nishio-Hamane, *Magnetic properties of Mn–Bi melt-spun ribbons*, *J. Magn. Magn. Mater.* **349** (2014) 9.
[14] P. Kharel, V. R. Shah, R. Skomski, J. E. Shield and D. J. Sellmyer *Magnetism of MnBi-Based Nanomaterials*, *IEEE Trans. Magn.* **49** (2013) 3318.
[15] K. Ishida and T. Nishizawa, *The Co-Mn (cobalt-manganese) system*, *Bull. Alloy Phase Diagr.* **11** (1990) 125.
[16] X. Guo, A. Zaluska, Z. Altounian and J. O. Ström-Olsen, *The formation of single-phase equiatomic MnBi by rapid solidification*, *J. Mater. Res.* **5** (1990) 2646.
[17] Truong Xuan Nguyen, Hai Van Pham, Vuong Van Nguyen, *Effect of Sb substitution on structural and magnetic properties of MnBi based alloys*, *Physica B Condens. Matter* **552** (2019) 190.
[18] Truong Xuan Nguyen, Oanh Kim Thi Vuong, Hieu Trung Nguyen and Vuong Van Nguyen, *Preparation and Magnetic Properties of MnBi/Co Nanocomposite Magnets*, *J. Electron. Mater.* **46** (2017) 3359.
[19] Vuong Van Nguyen and Truong Xuan Nguyen, *Effects of microstructures on the performance of rare-earth-free MnBi magnetic materials and magnets*, *Physica B: Condens. Matter* **532** (2018) 103.